



Nanotesla sensitivity magnetic field sensing using a compact diamond nitrogen-vacancy magnetometer

Webb, James Luke; Clement, Joshua David; Troise, Luca; Ahmadi, Sepehr; Johansen, Gustav Juhl; Huck, Alexander; Andersen, Ulrik Lund

Published in:
Applied Physics Letters

Link to article, DOI:
[10.1063/1.5095241](https://doi.org/10.1063/1.5095241)

Publication date:
2019

Document Version
Publisher's PDF, also known as Version of record

[Link back to DTU Orbit](#)

Citation (APA):
Webb, J. L., Clement, J. D., Troise, L., Ahmadi, S., Johansen, G. J., Huck, A., & Andersen, U. L. (2019). Nanotesla sensitivity magnetic field sensing using a compact diamond nitrogen-vacancy magnetometer. *Applied Physics Letters*, 114(23). <https://doi.org/10.1063/1.5095241>

General rights

Copyright and moral rights for the publications made accessible in the public portal are retained by the authors and/or other copyright owners and it is a condition of accessing publications that users recognise and abide by the legal requirements associated with these rights.




- Users may download and print one copy of any publication from the public portal for the purpose of private study or research.
- You may not further distribute the material or use it for any profit-making activity or commercial gain
- You may freely distribute the URL identifying the publication in the public portal

If you believe that this document breaches copyright please contact us providing details, and we will remove access to the work immediately and investigate your claim.

Nanotesla sensitivity magnetic field sensing using a compact diamond nitrogen-vacancy magnetometer **F**

Cite as: Appl. Phys. Lett. **114**, 231103 (2019); <https://doi.org/10.1063/1.5095241>

Submitted: 08 March 2019 . Accepted: 30 May 2019 . Published Online: 13 June 2019

James L. Webb , Joshua D. Clement, Luca Troise, Sepehr Ahmadi , Gustav Juhl Johansen, Alexander Huck , and Ulrik L. Andersen

COLLECTIONS

F This paper was selected as Featured



View Online



Export Citation



CrossMark

ARTICLES YOU MAY BE INTERESTED IN

[Dual-polarization analog optical phase conjugation for focusing light through scattering media](#)
Applied Physics Letters **114**, 231104 (2019); <https://doi.org/10.1063/1.5097181>

[Delta-doped SrTiO₃ top-gated field effect transistor](#)

Applied Physics Letters **114**, 231605 (2019); <https://doi.org/10.1063/1.5090269>

[Meandering growth of in-plane silicon nanowire springs](#)

Applied Physics Letters **114**, 233103 (2019); <https://doi.org/10.1063/1.5097429>

Lock-in Amplifiers up to 600 MHz

starting at

\$6,210



 Zurich Instruments

Watch the Video



Nanotesla sensitivity magnetic field sensing using a compact diamond nitrogen-vacancy magnetometer



Cite as: Appl. Phys. Lett. **114**, 231103 (2019); doi: [10.1063/1.5095241](https://doi.org/10.1063/1.5095241)

Submitted: 8 March 2019 · Accepted: 30 May 2019 ·

Published Online: 13 June 2019



View Online



Export Citation



CrossMark

James L. Webb, Joshua D. Clement, Luca Troise, Sepehr Ahmadi, Gustav Juhl Johansen, Alexander Huck, ^{a)} and Ulrik L. Andersen ^{b)}

AFFILIATIONS

Center for Macroscopic Quantum States (bigQ), Department of Physics, Technical University of Denmark, Fysikvej 309, 2800 Kgs. Lyngby, Denmark

^{a)}Electronic mail: alexander.huck@fysik.dtu.dk

^{b)}Electronic mail: ulrik.andersen@fysik.dtu.dk

ABSTRACT

Solid state sensors utilizing diamond nitrogen-vacancy (NV) centers are a promising sensing platform that can provide high sensitivity and spatial resolution at high precision. Such sensors have been realized in bulky laboratory-based forms; however, practical applications demand a miniaturized, portable sensor that can function in a wide range of environmental conditions. Here, we demonstrate such a diamond NV magnetic field sensor. The sensor head fits inside a $11 \times 7 \times 7 \text{ cm}^3$ 3D-printed box and exhibits sub-10 nT/ $\sqrt{\text{Hz}}$ sensitivity over a 125 Hz bandwidth. We achieve efficient fluorescence collection using an optical filter and diode in contact with the diamond, which is cut at the Brewster angle to maximize the coupling of 532 nm pump light. We discuss the potential of this flexible approach to achieve sub-nT/ $\sqrt{\text{Hz}}$ shot noise limited sensitivity suitable for detection of a wide range of low-level magnetic fields, particularly those from electrical power systems and from biological sources.

© 2019 Author(s). All article content, except where otherwise noted, is licensed under a Creative Commons Attribution (CC BY) license (<http://creativecommons.org/licenses/by/4.0/>). <https://doi.org/10.1063/1.5095241>

Quantum sensing using nitrogen-vacancy (NV) centers in diamond has attracted widespread interest in recent years due to the extraordinary high sensitivity and high precision sensory capability of materials under ambient conditions.¹ Sensing of electric fields,² temperature,³ strain fields,⁴ and pressure⁵ has been demonstrated. In particular, research has focused on detection of magnetic fields with a high spatial resolution down to the nanoscale^{6–8} and on samples in environmental conditions that cannot be addressed by alternative solid state magnetometers.

The sensing mechanism is based on electron spin resonance via optical detection of fluorescence from an ensemble of NV centers which is sensitive to local magnetic and electric fields, in addition to the background conditions (e.g., temperature). The sensor sensitivity depends on various parameters, in particular, the number of active NV centers and the spin coherence time T_2^* . These parameters depend on diamond type and the growth method: high pressure high temperature vs chemical vapor deposition, the isotopic composition of the diamond (purified ^{12}C vs ^{13}C), and the defect nitrogen isotope.⁹

Numerous studies on NV based sensors have focused on increasing the sensitivity via higher photon collection efficiency,^{10–12} using novel excitation schemes,^{13,14} optimized measurement protocols,¹⁵ and diamond structures.¹⁶ Most realizations have been large, bulky setups allowing for maximum optimization and sensitivity in a fixed position. However, as sensor sensitivity now approaches a stage where new interesting applications become possible (e.g., in biodiagnostics), it is of great importance to design and develop miniaturized and movable versions. Recent work has been dedicated to the development of rugged, stable, transportable, and miniaturized diamond sensors to realize such applications.^{17–19}

In this article, we present the design and construction of such a miniaturized, handheld diamond magnetic field sensor based on readily available off-the-shelf and 3D printed components. Using a specially cut and coated (but commercially available) diamond sample combined with a cheap microwave (MW) antenna, an optical filter, and a photodiode, we demonstrate a compact NV excitation and fluorescence collection strategy which in turn enables the construction of a

compact hand-held magnetometer head, coupled to an external microwave and laser source. We show that such a sensor can achieve $7 \text{ nT}/\sqrt{\text{Hz}}$ sensitivity over a bandwidth of 125 Hz, highly suitable for low field, low frequency sensing applications. A NV magnetometer measures external magnetic fields through the Zeeman shift of its spin-triplet 3A ground state ($m_s = 0, \pm 1$), as shown in Fig. 1. A magnetic field induces an energy shift in the ground triplet state of $m_s \gamma_e B_z$, where B_z is the magnetic field along an NV symmetry axis and γ_e is the gyromagnetic ratio (28 Hz/nT). A measurement of the $m_s = \pm 1$ NV ground state energy shift thus reveals information about the strength of the magnetic field along an NV axis.

The field-induced energy shift in the triplet is measured using the technique of optically detected magnetic resonance (ODMR), where the NV centers are both optically excited and driven by a microwave (MW) source. When driven with MW frequency corresponding to the spin splitting of the triplet state, relaxation can occur via a singlet state, as shown in Fig. 1. This results in a detectable dip in red $\approx 637 \text{ nm}$ fluorescence output at a frequency that depends on the Zeeman shift and hence the magnetic field. Intersystem crossing from the singlet shelving state to the $m_s = 0$ triplet ground state polarizes the spins in the $m_s = 0$ ground state. Under optical pumping with green laser light, this completes a loop that allows continuous detection of the ODMR fluorescence dip.²⁰ Detection of ODMR can be via a pulsed scheme, using a Ramsey or spin-echo sequence⁹ or, as in this work, a simpler, robust continuous wave (CW) approach with constant laser and MW power.

There are two primary obstacles to achieving high sensitivity in an NV-based sensor. First, it is necessary to efficiently excite the NV centers. The low NV center absorption cross section requires a high

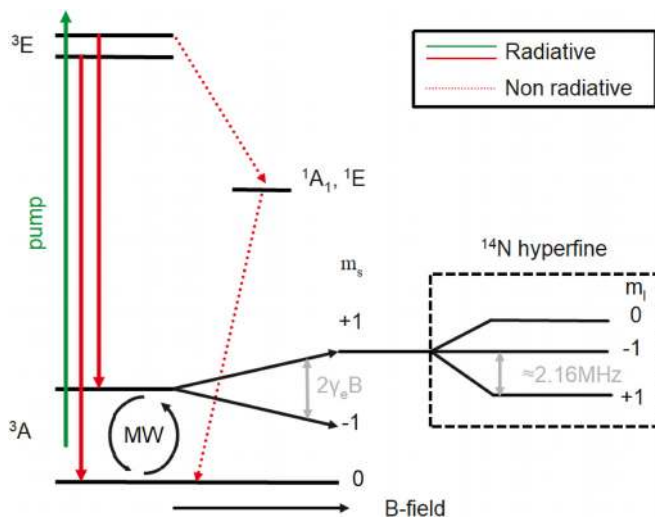


FIG. 1. NV energy level scheme. The NV center is optically pumped at 532 nm into the excited triplet state 3E and decays back into the ground state 3A with fluorescent red emission. For the $m_s = 0$ sublevel, emission occurs within the triplet only. For the $m_s = \pm 1$ levels, intersystem crossing into a singlet state 1E can lead to decay nonradiatively (or via 1042 nm infrared emission) via the singlet ground state 1A . This results in a dip in fluorescence output. By transferring the populations between $m_s = 0$ and $m_s = \pm 1$, through absorption of resonant MWs at $\approx 2.8 \text{ GHz}$, dependent on the Zeeman shift of the 3E levels, this drop in fluorescence can be directly observed (ODMR). The electronic transitions are hyperfine split by the ^{14}N nuclear spin.

power pump laser, pump trapping,¹³ or an optical cavity.²¹ Second, fluorescence light must be efficiently captured, despite the high refractive index of diamond meaning much of it is trapped by total internal reflection. Different schemes to maximize fluorescence collection include using a parabolic collection lens,¹² collection at the diamond edges,⁷ and using a dielectric antenna.¹¹

In this work, we have addressed these two challenges by using an approach with angled cut diamond end facets that allow a high power, tightly collimated pump beam to travel laterally through the entire diamond width. This is outlined schematically in Fig. 2(a). In addition, we maximize the collection of this light by attaching (using immersion oil) a photodiode to the front surface of the diamond after a thin optical filter while reflective coating the back.

The simplified and compact setup design is presented in Fig. 2(b). We used a commercially available single crystal diamond, grown via chemical vapor deposition with the natural ^{13}C content, with dimensions of $6 \times 6 \times 1.2 \text{ mm}^3$ from Element 6. The sample had $[^{14}\text{N}] < 1 \text{ ppm}$, and the natural $[^{14}\text{NV}]$ concentration was determined to be $\approx 0.2 \text{ ppb}$.²¹ We used a p-polarized pump laser (Cobolt 05-01) with a maximum power of 0.5 W at 532 nm, which can be fiber coupled into the sensor head. The pump beam was collimated to a mode field diameter of approximately $45 \mu\text{m}$ and focused on one of the edge cut facets of the diamond. The two edge facets for the 532 nm pump beam were cut by Almax easyLab to the Brewster angle of $67^\circ \pm 0.1^\circ$, respectively, facilitating efficient entry of the pump beam into the

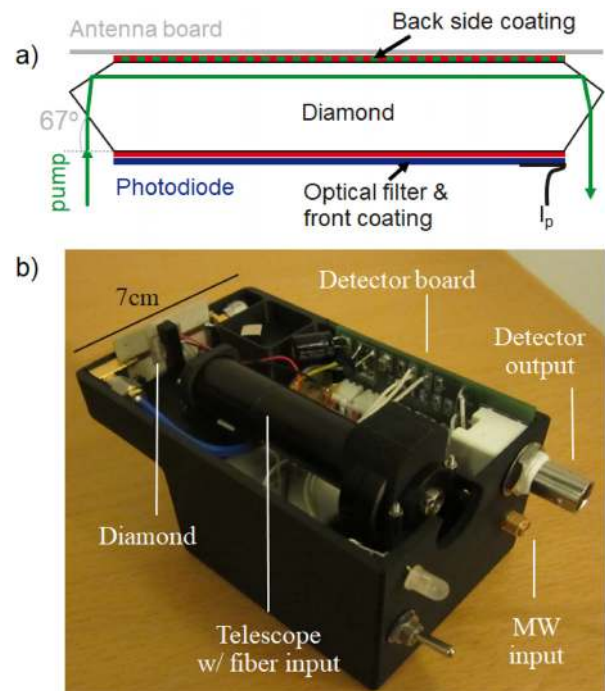


FIG. 2. (a) Schematic of the specially cut diamond crystal, optical coatings and filter, attached photodiode, and MW antenna. We use two cut surfaces, one at the diamond Brewster angle (67°) to ensure maximum transmission of a beam perpendicular to the diamond front surface and a second cut at 22.7° to direct the beam laterally through the entire width of the diamond, exciting the maximum number of NV centers as possible and exiting at an identically cut facet on the opposite side. (b) Labeled photograph of the opened handheld sensor head.

diamond. We estimate the pump beam to propagate inside at least the full width of the diamond (≈ 6 mm). As indicated in Fig. 2, the back side of the diamond was coated with a highly reflective (HR, $R > 99\%$) coating covering the spectrum 500–800 nm, while the front side was HR ($R > 99\%$) coated for 532 nm and antireflective coated ($R < 1\%$) for 600–800 nm. We attach a 550 nm long pass optical filter (Thorlabs FELH0550, cut to size) before the photodiode to reject stray pump light.

The diamond was mounted onto a printed circuit board with a MW split-ring resonator²² with a diamond loaded design resonance frequency of 2.89 GHz confirmed by a S_{11} reflection measurement. Microwaves were delivered from an external source (Stanford SG380 with Minicircuits ZHL-16W-43+ amplifier) at a 500 kHz width frequency modulation at 33.3 kHz. For the magnetic field measurements, we applied a MW drive with three frequency components separated by the ^{14}N hyperfine frequency of $f_{hf} = 2.16$ MHz to boost sensitivity.²¹

For optical detection, we used photodiodes (PDB-C160SMCT-ND, Advanced Photonix), 15 V battery reverse biased. The photodiode responsivity was $R_{532\text{ nm}} = 0.2$ A/W at 532 nm and $R_{637\text{ nm}} = 0.37$ A/W at 637 nm. By using a small polarizing beam splitter and half-wave plate, we sampled a fraction of the 532 nm pump laser beam and directed this onto a secondary, identical photodiode in a balanced detection scheme in order to perform common mode rejection (CMR) of pump laser technical noise. The resulting signal was passed into a lock-in amplifier (Stanford Research 850), external to the sensor head, locked to the MW modulation frequency (33.3 kHz), with output digitized by an external analog-to-digital converter (NI-DAQ 6221) allowing precise detection of the ODMR spectrum. We consider that in an updated design, these components could be readily incorporated in the sensor head.

We optimized our setup by first measuring the DC photocurrent I_{pc} directly using an ammeter from the primary photodiode on the diamond as a function of pump laser power from 30 mW up to 0.5 W. We also measured the amplitude spectral density (ASD) of the detected modulated ($f_m = 33.3$ kHz) fluorescence signal using only the primary photodiode and by CMR via balanced detection. This was done by a fast-Fourier transform of a 1 s signal digitized at 125 kSa/s, taking the average level up to the -3 dB filter roll-off imposed by the lock-in time constant (1 ms). The ASD as a function of I_{pc} can be seen in Fig. 3 alongside the shot noise level, calculated from the DC photocurrent, and the electronic noise floor. We define the electronic noise floor as the noise level from the detection electronics with zero pump and ambient illumination. The single and balanced photodiode data therefore include this electronic noise. The measurements demonstrate the dominance of technical noise from the pump laser over all other sources of noise. CMR of technical noise was able to reduce the noise level by $> \times 10$ vs single diode detection. Using CMR, we were able to obtain near shot noise limited fluorescence detection, the difference being due to the limitations of our manual (optical) balancing scheme. We measured photocurrent to scale linearly with pump power, indicating better photodetection sensitivity at high power (due to the scaling of shot noise with the root of laser power). Using maximum laser power (0.5 W), we then measured the ODMR spectrum from the diamond. In order to resolve the ^{14}N hyperfine structure, we use a fixed offset field ≈ 1 mT from two rare earth magnets. The optical magnetic resonance spectrum was recorded by sweeping the MW frequency, measuring the modulated photovoltage using a lock-in amplifier. The

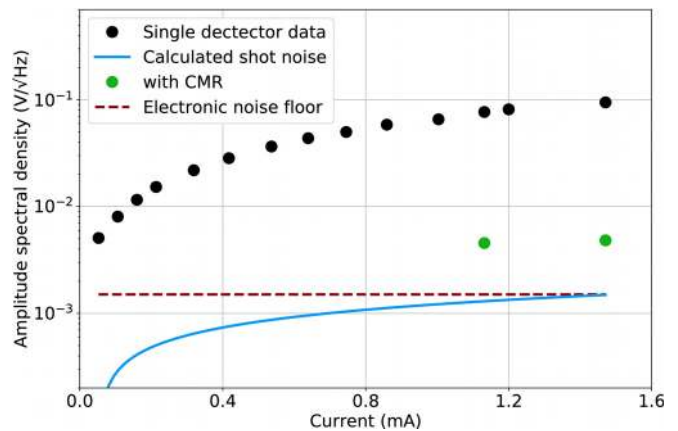


FIG. 3. Mean amplitude spectral density of the optical signal over the 125 Hz sensing bandwidth, plotted as a function of photocurrent, I_{pc} for a single photodiode (the primary photodiode on the diamond), at 330 mW and 0.5 W for two photodiodes in a balanced configuration to reject common mode noise (with CMR). We also plot the shot noise for a single detector calculated from I_{pc} ($\times \sqrt{2}$ for CMR) and the electronic noise floor.

plotted spectrum in Fig. 4 arises from the deliberate permanent magnet alignment along one of the four $\langle 111 \rangle$ NV axes and clearly shows the ^{14}N hyperfine splitting. By a linear fit to the ODMR spectrum, we determine a slope of $25 \mu\text{V}/\text{Hz}$ corresponding to 0.7 mV/nT assuming a shift of 28 Hz/nT . This slope was optimized by repeating the ODMR spectrum as a function of MW drive power. The optimum power prior to amplification was 4 dBm and -2 dBm for the main and 2.16 MHz drive, respectively, giving ≈ 6 W from the amplifier. We note importantly no saturation of the ODMR contrast with laser power, an issue that can limit NV sensor sensitivity.²³ With the sensitivity determined from the ODMR spectrum, we measured magnetic sensitivity as a function of magnetic field frequency, again by fast-

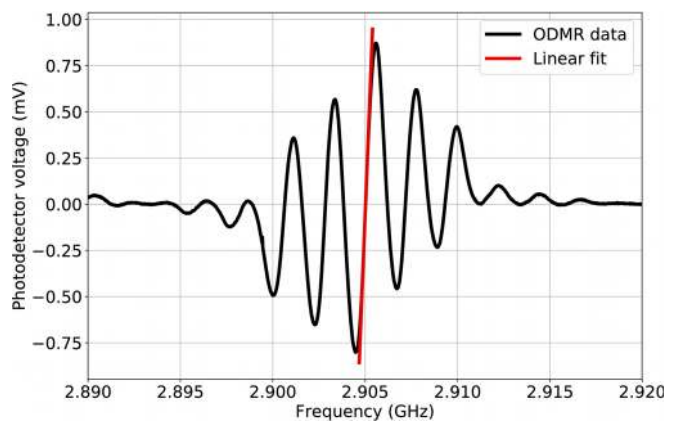


FIG. 4. Optically detected magnetic resonance (ODMR) spectrum, recorded as a function of MW drive frequency with CMR on. We observe the $m_s = 0 \leftrightarrow +1$ electron spin transition and hyperfine splitting arising from ^{14}N . By a linear fit to the slope of the ODMR spectrum, we determined the relation between signal voltage and frequency shift to be $25 \mu\text{V}/\text{Hz}$, from which we determined the magnetic field sensitivity using the relation $\gamma_e B_z$, assuming $\gamma_e = 28 \text{ Hz/nT}$.

Fourier transform of 1 s of digitized signal at 125 kSa/s. The magnetic noise density spectrum is plotted in Fig. 5. We compare sensitivity with CMR on and off and at MW drive frequencies of 2.905 GHz and 2.908 GHz, corresponding to the points of maximum (least) magnetic field sensitivity as determined from the maximum slope (peak) of the ODMR spectrum. We plot the ultimate electronic noise floor, defined by our amplifier and analog-to-digital converter, located at $\approx 2 \text{ nT}/\sqrt{\text{Hz}}$.

The amplitude spectrum shows a noise floor of $\approx 150 \text{ nT}/\sqrt{\text{Hz}}$ without CMR and $\approx 7 \text{ nT}/\sqrt{\text{Hz}}$ with CMR turned on. This highlights how essential rejection of laser technical noise is in diamond magnetometry. When magnetically sensitive, we observed peaks primarily at 50 Hz and 150 Hz. Such peaks were not observed when at a magnetically insensitive drive frequency (2.908 GHz). These frequencies correspond clearly to direct detection of the magnetic field produced by nearby electrical transformers: the strong 3rd harmonic at 150 Hz is a frequency component of the transformer magnetic field produced by magnetic hysteresis in the transformer core. Were we detecting spurious mains electrical noise, the 2nd harmonic at 100 Hz would also be strongly present. Peaks at 60 Hz and higher harmonics were traced to inbuilt components in United States-purchased equipment.

Based on the detected photocurrent, we calculate the total optical power detected by the primary photodiode to be 3.6 mW. This corresponds to an estimated shot noise limited sensitivity of $\approx 3 \text{ nT}/\sqrt{\text{Hz}}$. The absorption cross section at 532 nm for a single ^{14}NV center is reported²⁴ to be $\sigma_{\text{NV}} = 3.1 \times 10^{-15} \text{ mm}^2$. Taking a NV density of $6.4 \times 10^{13} \text{ cm}^{-3}$, a NV quantum efficiency of $\eta \approx 0.9$,²⁵ and a propagation length inside the diamond of 6 mm, the fluorescence power from the ensemble is 0.53 mW at the maximum pump power (0.5 W). This is significantly lower than the measured fluorescence power of 3.6 mW. This illustrates that the majority of the photocurrent is due to leakage of pump light past the filter and into the photodiode. It also highlights the minimal single pass absorption of the pump light by our diamond with this level of NV defects. Such absorption can be enhanced by

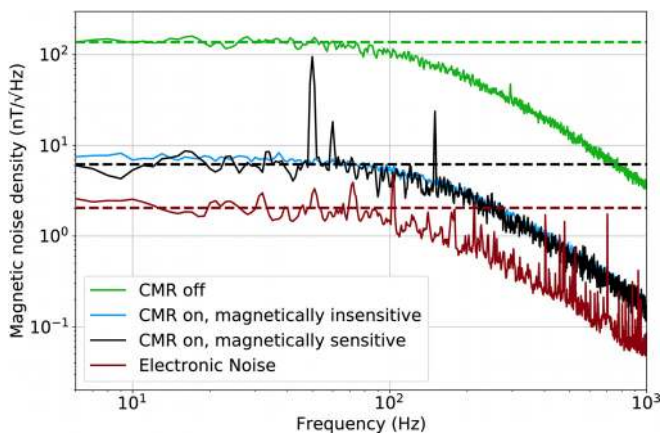


FIG. 5. Magnetic noise frequency spectrum at 0.5 W pump power, plotted as ASD in $\text{nT}/\sqrt{\text{Hz}}$. We show the noise density without balanced detection (CMR off), with CMR on and the detector magnetically sensitive (2.905 GHz) and insensitive (2.908 GHz). We also show the electronic limit (pump off). We observe a mean noise floor of $7 \text{ nT}/\sqrt{\text{Hz}}$ when rejecting laser technical noise. We observe the same high frequency peaks at 400–1 kHz on all data, from the power supplies and cooling fans. Only when magnetically sensitive do we clearly observe 50/150 Hz peaks from mains transformer field.

boosting defect density via optimized doping, irradiation, and annealing or by use of an optical cavity around the diamond.²⁵

Our current design has potential to be improved to subnanotesla sensitivity and in compactness and size. The primary limitation of our sensor head size was the internal focusing optics, which could be further miniaturized. Increasing the NV concentration in combination with ^{12}C purification has been shown to improve ODMR contrast and reduce linewidth.⁹ Leakage of pump light, in a wide range of incidence angles, proved difficult to fully reject in our sensor using available commercial filters. Further improvement in filter composition and structure is required in this geometry. Moving the filter away from the diamond surface to narrow the incidence angle of scattered pump light would help, but at the expense of sensor miniaturization. An ideal filter rejecting all pump light reduces the shot noise by approximately a factor of 2–3. Electronic balancing of the detection and CMR would reduce our electronic noise floor. In the shot noise limit, simply increasing laser power would improve sensitivity (3.3 W pump power has been demonstrated²⁶). We note that our bandwidth is not imposed by the physics of our sensor and could easily be increased in order to detect higher frequency fields, limited only by relaxation time T_2^* . A noise source not considered here is temperature variation, dependent on heat dissipation and the local environment. It has been demonstrated that such temperature effects can be efficiently corrected by driving simultaneously at both the $m_s = \pm 1$ MW resonances.²⁷

Several recent efforts have been made to produce a miniaturized NV magnetometer as an integrated package,^{18,19} with onboard light and MW sources, of sensitivity in the 30–100 $\text{nT}/\sqrt{\text{Hz}}$ range. We show that to achieve subnanotesla level sensitivity may require pump power of the order of several Watts for a millimeter-scale diamond with a sufficiently large NV ensemble at currently achievable NV defect densities and levels of material strain. This factor suggests that having a sensor head(/s) into which laser and MWs can be coupled (a setup common in, e.g., medical devices) may be preferable for high sensitivity operation, since it may be difficult to generate enough power at low electronic noise in an integrated package within the sensor head.

The level of sensitivity we demonstrate in this work should permit many new applications. We particularly highlight applications in sensing of weak (nanotesla, picotesla scale) magnetic fields from biological sources, such as living tissue or samples in solution. This can be difficult for alternative techniques, e.g., unencapsulated magnetoresistive sensors, relying on electrical readout. Biocompatibility of diamond allows high proximity with a sample, assisting field detection given the rapid (cubic) drop in field strength with distance. Competing techniques may need to be positioned relatively far (many millimeters) from the sample. Of particular interest is sensing of bioelectric signals by their magnetic field that cannot otherwise be easily accessed by electrical probes (for example, magnetoencephalography of the brain) where current magnetometers—superconducting quantum interference (SQUID) devices or recently demonstrated atomic vapor cells²⁸—are expensive and cumbersome and have poor spatial resolution.

High spatial resolution in diamond NV sensors can be readily achieved by imaging fluorescence with a camera and has been demonstrated elsewhere in, e.g., geological samples²⁹ and magnetic bacteria to the micrometer scale.³⁰ Biological signals are typically observed in the hundreds of hertz to low-kilohertz frequency range, over which we demonstrate excellent sensitivity in this work. Other low frequency

magnetic signals of interest include diagnostics of mains power systems (transformers, motors) operating at DC or single/three phase 50/60 Hz.

In conclusion, we have developed a diamond magnetometer with a handheld sensing head, with a sensitivity of $7 \text{ nT}/\sqrt{\text{Hz}}$ and an ultimate noise floor of $3 \text{ nT}/\sqrt{\text{Hz}}$. We demonstrate robust, flexible sensing using diamond NV centers which is not limited to fixed benchtop applications. We discuss a route to achieving sub- $\text{nT}/\sqrt{\text{Hz}}$ sensitivity through improvements in the NV-concentration, optical filtering, and detection and by implementing pulsed measurement schemes.

We gratefully acknowledge Kristian H. Rasmussen and Aleksander Tchernavskij for support in fabrication and electronic design. This project was financially supported by the Innovation Fund Denmark (EXMAD project and Qubiz center) and the Novo Nordisk foundation (bioQ project).

REFERENCES

- ¹J. M. Taylor, P. Cappellaro, L. Childress, L. Jiang, D. Budker, P. R. Hemmer, A. Yacoby, R. Walsworth, and M. D. Lukin, *Nat. Phys.* **4**, 810 (2008).
- ²F. Dolde, H. Fedder, M. W. Doherty, T. Noebauer, F. Remppl, G. Balasubramanian, T. Wolf, F. Reinhard, L. C. L. Hollenberg, F. Jelezko, J. Wrachtrup, and T. Nöbauer, *Nat. Phys.* **7**, 459 (2011).
- ³V. M. Acosta, E. Bauch, M. P. Ledbetter, A. Waxman, L.-S. Bouchard, and D. Budker, *Phys. Rev. Lett.* **104**, 070801 (2010).
- ⁴M. E. Trusheim and D. Englund, *New J. Phys.* **18**, 123023 (2016).
- ⁵M. W. Doherty, V. V. Struzhkin, D. A. Simpson, L. P. McGuinness, Y. Meng, A. Stacey, T. J. Karle, R. J. Hemley, N. B. Manson, L. C. Hollenberg, and S. Praver, *Phys. Rev. Lett.* **112**, 047601 (2014).
- ⁶P. Maletinsky, S. Hong, M. S. Grinolds, B. Hausmann, M. D. Lukin, R. L. Walsworth, M. Loncar, and A. Yacoby, *Nat. Nanotechnol.* **7**, 320 (2012).
- ⁷D. Le Sage, L. M. Pham, N. Bar-Gill, C. Belthangady, M. D. Lukin, A. Yacoby, and R. L. Walsworth, *Phys. Rev. B* **85**, 121202 (2012).
- ⁸K. Jensen, V. M. Acosta, A. Jarmola, and D. Budker, *Phys. Rev. B* **87**, 014115 (2013).
- ⁹L. Rondin, J.-P. Tetienne, T. Hingant, J.-F. Roch, P. Maletinsky, and V. Jacques, *Rep. Prog. Phys.* **77**, 056503 (2014).
- ¹⁰L. Marseglia, J. P. Hadden, A. Stanley-Clarke, J. P. Harrison, B. Patton, Y.-L. D. Ho, B. Naydenov, F. Jelezko, J. Meijer, P. R. Dolan, J. M. Smith, J. G. Rarity, and J. L. O'Brien, *Appl. Phys. Lett.* **98**, 133107 (2011).
- ¹¹D. Riedel, D. Rohner, M. Ganzhorn, T. Kaldewey, P. Appel, E. Neu, R. Warburton, and P. Maletinsky, *Phys. Rev. Appl.* **2**, 064011 (2014).
- ¹²T. Wolf, P. Neumann, K. Nakamura, H. Sumiya, T. Ohshima, J. Isoya, and J. Wrachtrup, *Phys. Rev. X* **5**, 041001 (2015).
- ¹³H. Clevenson, M. E. Trusheim, C. Teale, T. Schröder, D. Braje, and D. Englund, *Nat. Phys.* **11**, 393 (2015).
- ¹⁴L. Bougas, A. Wilzewski, Y. Dumeige, D. Antypas, T. Wu, A. Wickenbrock, E. Bourgeois, M. Nesladek, H. Clevenson, D. Braje, D. Englund, and D. Budker, *Micromachines* **9**, 276 (2018).
- ¹⁵V. M. Acosta, E. Bauch, A. Jarmola, L. J. Zipp, M. P. Ledbetter, and D. Budker, *Appl. Phys. Lett.* **97**, 174104 (2010).
- ¹⁶G. Balasubramanian, P. Neumann, D. Twitchen, M. Markham, R. Kolesov, N. Mizuochi, J. Isoya, J. Achard, J. Beck, J. Tessler, V. Jacques, P. R. Hemmer, F. Jelezko, and J. Wrachtrup, *Nat. Mater.* **8**, 383 (2009).
- ¹⁷G. Chatzidrosos, A. Wickenbrock, L. Bougas, N. Leefer, T. Wu, K. Jensen, Y. Dumeige, and D. Budker, *Phys. Rev. Appl.* **8**, 044019 (2017).
- ¹⁸F. M. Strner, A. Brenneis, J. Kassel, U. Wostradowski, R. Rlver, T. Fuchs, K. Nakamura, H. Sumiya, S. Onoda, J. Isoya, and F. Jelezko, *Diamond Relat. Mater.* **93**, 59 (2019).
- ¹⁹M. I. Ibrahim, C. Foy, D. Kim, D. R. Englund, and R. Han, in *2018 IEEE Symposium on VLSI Circuits* (2018), pp. 249–250.
- ²⁰G. M. H. Thiering and A. Gali, *Phys. Rev. B* **98**, 085207 (2018).
- ²¹S. Ahmadi, H. A. R. El-Ella, J. O. Hansen, A. Huck, and U. L. Andersen, *Phys. Rev. Appl.* **8**, 034001 (2017).
- ²²K. Bayat, J. Choy, M. Farrokh Baroughi, S. Meesala, and M. Loncar, *Nano Lett.* **14**, 1208 (2014).
- ²³A. Dréau, M. Lesik, L. Rondin, P. Spinicelli, O. Arcizet, J.-F. Roch, and V. Jacques, *Phys. Rev. B* **84**, 195204 (2011).
- ²⁴T.-L. Wee, Y.-K. Tzeng, C.-C. Han, H.-C. Chang, W. Fann, J.-H. Hsu, K.-M. Chen, and Y.-C. Yu, *J. Phys. Chem. A* **111**, 9379 (2007).
- ²⁵S. Ahmadi, H. A. R. El-Ella, A. M. Wojciechowski, T. Gehring, J. O. B. Hansen, A. Huck, and U. L. Andersen, *Phys. Rev. B* **97**, 024105 (2018).
- ²⁶J. M. Schloss, J. F. Barry, M. J. Turner, and R. L. Walsworth, *Phys. Rev. Appl.* **10**, 034044 (2018).
- ²⁷A. M. Wojciechowski, M. Karadas, C. Osterkamp, S. Jankuhn, J. Meijer, F. Jelezko, A. Huck, and U. L. Andersen, *Appl. Phys. Lett.* **113**, 013502 (2018).
- ²⁸E. Boto, N. Holmes, J. Leggett, G. Roberts, V. Shah, S. S. Meyer, L. D. Muñoz, K. J. Mullinger, T. M. Tierney, S. Bestmann, G. R. Barnes, R. Bowtell, and M. J. Brookes, *Nature* **555**, 657 (2018).
- ²⁹D. R. Glenn, R. R. Fu, P. Kehayias, D. Le Sage, E. A. Lima, B. P. Weiss, and R. L. Walsworth, *Geochem., Geophys., Geosyst.* **18**, 3254, <https://doi.org/10.1002/2017GC006946> (2017).
- ³⁰D. Le Sage, K. Arai, D. R. Glenn, S. J. Devience, L. M. Pham, L. Rahn-Lee, M. D. Lukin, A. Yacoby, A. Komeili, and R. L. Walsworth, *Nature* **496**, 486 (2013).